

# Transversal magneto-optical Kerr effect in three-periodic bigyrotropic photonic crystals

© I.A. Glukhov<sup>1,2,3</sup>, I.S. Panyayev<sup>1,2,¶</sup>, D.G. Sannikov<sup>1,2</sup>, Yu.S. Dadoenkova<sup>4</sup>, N.N. Dadoenkova<sup>1</sup>

<sup>1</sup> Donetsk Institute of Physics and Technology named after. A.A. Galkina, Donetsk, Russia

<sup>2</sup> Ulyanovsk State University, Ulyanovsk, Russia

<sup>3</sup> Kotel'nikov Institute of Radio Engineering and Electronics (Ulyanovsk Branch), Russian Academy of Sciences, Ulyanovsk, Russia

<sup>4</sup> École Nationale d'Ingénieurs de Brest, IRDL, UMR CNRS 6027, Brest, F-29000, France

¶e-mail: panyayev.ivan@rambler.ru

Received April 25, 2024

Revised April 25, 2024

Accepted May 20, 2024

We study one-dimensional three-periodic photonic crystal structures based on dielectrics (SiO<sub>2</sub>, TiO<sub>2</sub>) and ferrite garnets (YIG, Bi:YIG), forming supercells of the type  $[(ab)^N(cd)^M]^K$ . Using the  $4 \times 4$  matrix method, the frequency-angular spectra of plane electromagnetic waves of orthogonal polarizations are studied, and a comparative analysis of photonic band gaps for non-magnetic and magnetic photonic crystals and their combinations are carried out. The transverse (equatorial) magneto-optical Kerr effect, which occurs under 180°-magnetization reversal of the structures under consideration, has been studied. The applied aspect of using the results to create magnetically active optoelectronic components and nanophotonics devices operating in the infrared range is discussed.

**Keywords:** transversal magneto-optical Kerr effect, photonic band gap (PBG), photonic crystals (PCs).

DOI: 10.61011/EOS.2024.05.59123.6401-24

## 1. Introduction

Photonic crystals (PC) are artificial periodic structures with a period of the order of the electromagnetic radiation wavelength. During several decades, PCs have been the objects of intensive research and widely used in such areas as optoelectronics, spintronics, photonics due to their unique physical properties [1–5]. A characteristic feature of a PC is the presence of photonic band gaps (PBGs) — frequency (wavelength) ranges where the propagation of electromagnetic radiation inside the structure is impossible. The simplest example of a PC is a one-dimensional (1D) two-component periodic system where alternating layers of different materials  $a$  and  $b$  are repeated  $N$  times forming a finite structure  $(ab)^N$ .

Breaking of the PC periodicity leads to appearance of narrow transmission bands inside the PBG — intraband defect modes, which allows to use the PCs as narrow-band frequency filters and sensors. PCs with a complex structure of the unit cell on the base of three and more different materials forming periodic subsystems inside the unit cell are of special interest. Such PCs have a modified structure of PBGs where sets of narrow peaks as well as transmission bands can exist in different variations [6–10]. Advantages of such structures compared with „classical“ 1D PCs are the possibility of easier PBG tuning to the specified frequency ranges and the presence of intraband modes that which are narrower in frequency, etc.

PC structures with two periods where the internal block  $(ab)^N$  is inside the unit cell  $[(ab)^Nc]$ , repeating  $M$  times,

were treated as photonic-magnonic crystals [11–15] and as photonic hypercrystals [16–19]. In paper [20] the intraband modes in the near infrared transmission spectra of the  $(abc)^N$  type ternary PC structure are investigated. Paper [21] proposes a ternary „Si/polymer/SiO<sub>2</sub>“ PC structure as a temperature sensor. The operating principle of the proposed devices is based on the red shift of the transmission peak with the increase of temperature due to the thermo-optic effect and thermal expansion of the polymer. Ternary PC containing a superconductor has the same operating principle [22]. 1D PC biosensors can achieve more than double increase of the volumetric and surface sensitivity compared with conventional micromirror sensors [23]. Ternary 1D PC can be used in highly sensitive defect mode refractometric sensors [24].

When using functional materials, i.e. media whose properties can be controlled through external sources (electric and magnetic fields, pressure, temperature, etc.), additional possibilities appear to adjust optical properties of the PC structure components. Structures based on magnetic media are one of the classes of such structures that have been widely and successfully used over the last two decades. The interest in magneto-optical (MO) materials is justified by the presence of effects that change the polarization state and/or intensity of the interacting electromagnetic waves (EMWs), which is used in various photonic devices (switches, optical insulators, phase shifters, etc.). Depending on the mutual orientation of the wave vector of the EMW reflected from a MO structure and the magnetization vector direction, one

can distinguish the polar, the longitudinal (meridional), and the transverse (equatorial) MO Kerr effects. Thus, the transverse MO Kerr effect leads to a change in the intensity of light reflected from a magnetic material during the magnetization inverse. Therefore, it is widely used to study magnetic properties of media, to determine the parameters of ultrathin ferromagnetic films [25] and also can be used in data storage devices [26]. This effect can also occur in magneto-plasmonic structures [27] and, besides the properties of a MO material, can depend on other factors. For example, mismatch strains that occur in the vicinity of the geometrical boundary of a magnetic dielectric film — yttrium-iron garnet (YIG)  $\text{Y}_3\text{Fe}_5\text{O}_{12}$  - epitaxially grown on a gadolinium-gallium garnet substrate can cause a significant transverse MO Kerr effect which is negligibly low when there are no in absence of the strain [28].

So far, there is a large number of works on PCs containing magnetic bigyrotropic garnets and their varieties, in particular, bismuth-substituted YIG (Bi:YIG), cerium-substituted YIG (Ce:YIG), etc. [29,30]. Propagation of light in MO structures containing randomly distributed layers of Bi:YIG and  $\text{SiO}_2$  is analyzed by the transfer matrix method in [31]. The papers [11–15] have addressed photonic-magnonic crystals — biperiodic magnetic PCs functioning simultaneously for electromagnetic waves and spin waves, however, MO effects have not been investigated, with the exception of [15], where the peculiarities of the Faraday rotation in these structures have been studied.

This work describes theoretical studies of the  $[(ab)^N(cd)^M]^K$  type three-periodic 1D PC consisting of dielectrics ( $\text{SiO}_2$ ,  $\text{TiO}_2$ ) and bigyrotropic iron garnets (YIG, Bi:YIG). We discuss frequency spectra of EMWs, in dependence on the incidence angle, for the given type of the PC, optimal combinations of layers and layer thicknesses for the PBG tuning, as well as application opportunities of the transverse MO Kerr effect for the development of modern nanophotonic devices.

## 2. Problem formulation

Let us consider the  $[(ab)^N(cd)^M]^K$  type three-periodic PC (Figure 1) formed by a supercell repeated  $K$  times. The supercell is a combination of two multilayer  $(ab)^N$  and  $(cd)^M$  structures consisting of different materials  $a, b, c, d$ . The thicknesses of  $(ab)$  and  $(cd)$  subcells are denoted as  $L_1 = l_a + l_b$  and  $L_2 = l_c + l_d$ , and the supercell thickness (superperiod) is equal to  $L_3 = NL_1 + ML_2$  so that the total structure thickness is equal to  $KL_3$ . PC layers are arranged parallel to the  $(xy)$  plane. It is assumed that the longitudinal dimensions of PC (along the  $x$  and  $y$  axes) are quite large so that the boundary effects in these directions can be neglected. Layer thicknesses in the  $(ab)$  and  $(cd)$  subcells are chosen according to the Bragg's condition:  $n_{a,b}l_{a,b} = \lambda_{01}/4$  and  $n_{c,d}l_{c,d} = \lambda_{02}/4$ , where  $\lambda_{01}$  and  $\lambda_{02}$  are the Bragg wavelengths of the  $(ab)$  and  $(cd)$  subcells,

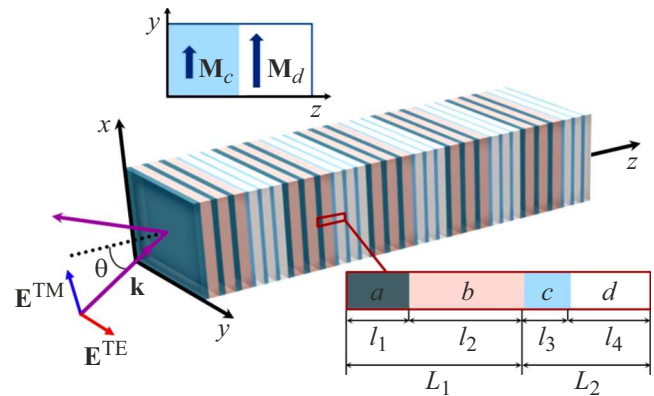


**Figure 1.** Schematic of  $[(ab)^N(cd)^M]^K$  three-periodic magneto-optical PC structure for  $N = 3$ ,  $M = 3$  and  $K = 5$ . Arrows in the top inset show the magnetization vectors  $\mathbf{M}_c$  and  $\mathbf{M}_d$  of the magnetic layers, the bottom inset shows the thicknesses of layers  $a, b, c, d$  that form the PC.

respectively,  $n_{a,b,c,d}$  are the refractive indices of layers at the corresponding Bragg's wavelength.

TE- or TM-polarized plane EMW with the angular frequency  $\omega$  and the wave vector  $\mathbf{k}$  impinges the PC surface in the incoming medium under the angle  $\theta$ , so that the  $(xz)$  plane is the plane of incidence. PC subcells can be formed from four layers  $a, b, c, d$  in different ways. However, below, we restrict ourselves with the case when the first  $(ab)$  cell consists of dielectric non-magnetic  $\text{SiO}_2$  and  $\text{TiO}_2$  layers, and the second  $(cd)$  cell consists of bigyrotropic YIG and Bi:YIG layers. All chosen materials are transparent in near IR range and are characterized by real values of dielectric permittivities  $\varepsilon_j$  (here  $j = in, a, b, c, d, out$ , whereas the incoming and outgoing media (air) are denoted as  $in$  and  $out$ ). As it will be shown below, such a choice of the materials allows us to obtain a sufficiently wide PBG with a system of narrow intraband transmission peaks [6].

We consider the transverse MO configuration, where a permanent magnetization field is applied along (or opposite to) the  $y$  axis, and the YIG and Bi:YIG layers have the saturation magnetizations  $|\mathbf{M}_c|$  and  $|\mathbf{M}_d|$ , respectively. Taking into account the first-order terms in the magnetization vector components, dielectric permittivity and magnetic susceptibility tensors are written as [26]:

$$\hat{\varepsilon} = \begin{pmatrix} \varepsilon & 0 & i\varepsilon' \\ 0 & \varepsilon & 0 \\ -i\varepsilon' & 0 & \varepsilon \end{pmatrix}, \quad \hat{\mu} = \begin{pmatrix} \mu & 0 & i\mu' \\ 0 & \mu & 0 \\ -i\mu' & 0 & \mu \end{pmatrix}. \quad (1)$$

Note that the off-diagonal components of the tensors  $\hat{\varepsilon}$  and  $\hat{\mu}$  are magnetically-induced and responsible for bigyrotropic properties of the chosen iron garnets.

## 3. Theory

The wave field components  $\mathbf{E}$  and  $\mathbf{H}$  of incident plane EMW with the frequency  $\omega$  are proportional

to  $\exp[i(\omega t - k_x x - k_z z)]$ , where  $k_x = k_0 \sin \theta$  (propagation constant) and  $k_z = k_0 \cos \theta$  are the wave vector projections on the  $x$  and  $z$  axes, respectively, and  $k_0 = 2\pi/\lambda$  is the wave number of EMW in vacuum. The transverse magnetization of the magnetoactive layers and the wave field homogeneity along the  $y$  axis lead to the separation of eigenstate EMW into TE- and TM-modes with the wave field components  $\{H_x, E_y, H_z\}$  and  $\{E_x, H_y, E_z\}$ .

For TE-modes, the tangential electric field component  $E_y$  in the  $j$ -th medium is

$$E_{y_j}(z) = F_j \exp(-ik_{z_j}z) + B_j \exp(ik_{z_j}z), \quad (2)$$

where  $F_j$  and  $B_j$  are the amplitudes of the „forward“ and „backward“ waves propagating along and opposite to the  $z$  axis (taking into account the chosen time-dependence of the EMW field on the time  $\exp(i\omega t)$ ),  $k_{z_j} = k_0 \sqrt{\varepsilon_j \mu_j - k_x^2}$  are  $z$ -components of the wave vectors which are the same for the TE- and TM-modes in the isotropic medium.

The tangential magnetic field component  $H_x$  of the TE-mode is written as:

$$H_{x_j}(z) = [\gamma_{\mu_j}^- F_j \exp(-ik_{z_j}z) + \gamma_{\mu_j}^+ B_j \exp(ik_{z_j}z)], \quad (3)$$

where  $\gamma_{\mu_j} = k_{z_j}/k_0 \mu_j$  with  $j$  corresponding to  $\text{TiO}_2$  and  $\text{SiO}_2$ , and

$$\gamma_{\mu_j}^{\pm} = \pm \frac{\mu_j k_{z_j} + i\mu_j' k_x}{k_0(\mu_j^2 - \mu_j'^2)}$$

for Bi:YIG and YIG. There is no reflected wave in the outgoing medium, therefore  $B_{out} = 0$  in contrast to the incoming medium where the corresponding coefficient is  $B_{in} \neq 0$ . For the TM-modes, the tangential electric and magnetic field components  $E_{x_j}(z)$  and  $H_{y_j}(z)$  are written similar to the expressions (2) and (3) with the field amplitude  $\tilde{F}_j$  and  $\tilde{B}_j$  and with the coefficients  $\gamma_{\mu_j}$  and  $\gamma_{\mu_j}^{\pm}$  replaced with the corresponding expressions  $\gamma_{\varepsilon_j} = k_{z_j}/k_0 \varepsilon_j$  and

$$\gamma_{\varepsilon_j}^{\pm} = \pm \frac{\varepsilon_j k_{z_j} + i\varepsilon_j' k_x}{k_0(\varepsilon_j^2 - \varepsilon_j'^2)}.$$

To obtain the transmission (reflection) coefficients of the electromagnetic modes, the standard  $(4 \times 4)$  transfer matrix method is used [32]. For convenient writing of the continuity equations for the tangential wave field components ( $E_x, E_y, H_x, H_y$ ) at the interfaces of all media, a field amplitude column vector  $\Psi_j = (F_j B_j \tilde{F}_j \tilde{B}_j)^T$  is introduced (here  $\tau$  is the transposition operation). Sequential exclusion of the field amplitudes at the internal interfaces of PC gives a transition to a set of four algebraic equations connecting the fields in air on the opposite sides of PC which can be written as:

$$\Psi_{out}(KL_3) = \hat{E}_{out}^{-1}(KL_3) \hat{S}_{out,a} \hat{G}_{a,in} \Psi_{in}. \quad (4)$$

Here,  $\hat{G}$  is the  $(4 \times 4)$  transfer matrix for the supercell:

$$\hat{G} = \hat{S}_{ac} \hat{T}_{cd}^M \hat{S}_{ca} \hat{T}_{ab}^N. \quad (5)$$

Here,  $\hat{T}$  are transfer matrices for the  $(ab)$  and  $(cd)$  subcells defined by the following expressions:

$$\begin{aligned} \hat{T}_{ab} &= \hat{S}_{ab} \hat{E}_b(l_b) \hat{S}_{ba} \hat{E}_a(l_a), \\ \hat{T}_{cd} &= \hat{S}_{cd} \hat{E}_d(l_d) \hat{S}_{dc} \hat{E}_c(l_c), \end{aligned} \quad (6)$$

where the matrices  $S_{ij} = \hat{A}_i^{-1} \hat{A}_j$  connecting the wave field amplitudes at the interface of layers  $i$  and  $j$  have a quasideagonal form

$$\hat{A}_j = \begin{bmatrix} \hat{A}_j^{(\text{TE})} & \hat{O} \\ \hat{O} & \hat{A}_j^{(\text{TM})} \end{bmatrix}.$$

$\hat{O}$  are zero matrices  $(2 \times 2)$ , and the coefficient matrices  $A_j^{(\text{TE})}, A_j^{(\text{TM})}$  for TE- and TM-modes are written as

$$\hat{A}_j^{(\text{TE})} = \begin{bmatrix} 1 & 1 \\ \gamma_{\mu_j} & -\gamma_{\mu_j} \end{bmatrix}, \quad \hat{A}_j^{(\text{TM})} = \begin{bmatrix} 1 & 1 \\ \gamma_{\varepsilon_j} & -\gamma_{\varepsilon_j} \end{bmatrix}. \quad (7)$$

Diagonal matrices in equations (6)

$$\begin{aligned} \hat{E}_j(l_j) &= \text{diag}[\exp(-ik_{z_j}l_j), \exp(ik_{z_j}l_j), \\ &\quad \exp(-ik_{z_j}l_j), \exp(ik_{z_j}l_j)] \end{aligned} \quad (8)$$

characterize the phase incursion inside the layer  $j$  with the thickness  $l_j$ . For detailed description of the transfer matrix method, see, for example, study [32]. The transmission coefficients  $T^{(\text{TE})}$  and  $T^{(\text{TM})}$  the reflection coefficients  $R^{(\text{TE})}$  and  $R^{(\text{TM})}$  are determined as follows:

$$T^{(\text{TE})} = |F_{out}|^2 / |F_{in}|^2, \quad T^{(\text{TM})} = |\tilde{F}_{out}|^2 / |\tilde{F}_{in}|^2, \quad (9)$$

whereby without absorption

$$R^{(\text{TE}),(\text{TM})} = 1 - T^{(\text{TE}),(\text{TM})}. \quad (10)$$

The value of the transverse MO Kerr effect can be determined in different ways, for example, in a way similar to the optical contrast [33,34]. In this work, the transverse MO Kerr effect parameter is determined as

$$\delta = \frac{R^+ - R^-}{R^+ + R^-}, \quad (11)$$

where  $R^{\pm}$  is the energy reflection coefficient for PC whose magnetic layers are magnetized along the  $y$  axis („+“) and opposite to the  $y$  axis („-“), respectively.

## 4. Numerical analysis and discussion

Let us assume that the energy of the incident EMW is not too high, therefore nonlinear effects which can occur in the structure at high intensities can be neglected. Dielectric permittivities and magnetic permeabilities of materials are given in the table. Since the frequency dispersion of the constitutive parameters of the system affects its optical

Dielectric permittivity and magnetic permeability of materials (parameters of equation (1))

| constitutive parameter | Material                                     |  |   |                                 |
|------------------------|--|--|---|---------------------------------|
|                        | TiO <sub>2</sub>                             | SiO <sub>2</sub>                             | YIG   | Bi:YIG                          |
| $\varepsilon$          | $\varepsilon_{\text{TiO}_2}(\lambda)$ , [35] | $\varepsilon_{\text{SiO}_2}(\lambda)$ , [36] | $\varepsilon_{\text{YIG}}(\lambda)$ , [37]                    | 5.76 [38], [39]*                |
| $\varepsilon'$         | 0  | 0  | $-2.47 \cdot 10^{-4}$ ( $\lambda = 1.152 \mu\text{m}$ , [40]) | 0.005 [38]                      |
| $\mu$                  | 1  | 1  | 1   | 1                               |
| $\mu'$                 | 0  | 0  | $8.76 \cdot 10^{-5}$ ( $\lambda = 1.152 \mu\text{m}$ , [40])  | $1.65 \cdot 10^{-5}$ [41], [42] |

Note. \* The chosen refractive index for Bi:YIG is close to the conventional value, for example, for Lu<sub>3-x</sub>Bi<sub>x</sub>Fe<sub>5</sub>O<sub>12</sub> ( $n = 2.33$ ) samples, and strongly depends on the concentration of bismuth.

response, the permittivity dispersion is taken into account. For the Bi:YIG layers, the off-diagonal component of the dielectric permittivity tensor can be determined as follows:  $\varepsilon' \approx 2\theta_F n_{\text{Bi:YIG}}/k_0$ , where  $\theta_F$  is the specific Faraday rotation angle, and  $n_{\text{Bi:YIG}}$  is the effective refractive index. It should be noted that minor frequency dispersion of the off-diagonal dielectric permittivity and magnetic permeability tensor elements of materials are neglected.

#### 4.1. Reflection spectra

The theoretical method described in Section 3 is applied to the calculations of frequency dependences of the EMW reflection coefficients for the three-periodic PC structure in the first PBG area. Note that the PC spectra strongly depend on the materials of the layers and their combinations, which has been studied in our work [6]. As three-periodic PC, the  $[(\text{SiO}_2/\text{TiO}_2)^N(\text{YIG}/\text{Bi:YIG})^M]^K$  structure is chosen where the first (nonmagnetic) pair of materials (SiO<sub>2</sub>/TiO<sub>2</sub>) is characterized by a significantly high optical contrast compared with the second (magnetic) pair (YIG/Bi:YIG). Thus, the SiO<sub>2</sub> layer is the first layer on which the EMW falls.

First, it makes sense to compare the reflection spectra of simple single-periodic PCs (SiO<sub>2</sub>/TiO<sub>2</sub>)<sup>NK</sup> and (YIG/Bi:YIG)<sup>MK</sup> which form a complex system, and a resulting three-periodic quaternary PC based on them.

Figure 2 shows the frequency-angle dependences of the reflection spectra for TE- and TM-modes (left and right columns, respectively) in the PC with the number of layers  $N = 3$ ,  $M = 10$ ,  $K = 3$ . Period number  $N$ ,  $M$  and superperiod number  $K$  are chosen to ensure the formation of pronounced PBGs with sharp edges for each single-period PC. The first and second rows show the single-periodic PC spectra: dielectric PC  $[(\text{SiO}_2/\text{TiO}_2)]^{NK}$  and bigyrotropic PC  $[(\text{YIG}/\text{Bi:YIG})]^{MK}$ , respectively, and the third row shows the quaternary PC spectra  $[(\text{SiO}_2/\text{TiO}_2)^N(\text{YIG}/\text{Bi:YIG})^M]^K$ . In [6], it has been shown that the behavior of the transmission spectra (position, width and sharpness of the PBGs boundaries and intraband modes) of three-periodic PCs depends significantly on the Bragg's wavelength tuning for each of the subcells (non-magnetic and magnetic), i.e. on  $\lambda_{01}$  and  $\lambda_{02}$ . Here the layer thicknesses are

chosen so that the quarter-wave condition is satisfied for  $\lambda_{01} = \lambda_{02} = 1.55 \mu\text{m}$ . For the dielectric PC, a sharp PBG is formed with a less number of layers (i.e.  $NK = 9$ ) than for the bigyrotropic PC ( $MK = 30$ ) due to a lower optical contrast of the YIG/Bi:YIG layers.

Let us first discuss the spectral characteristics inherent in all the structures studied. Light regions of the spectra correspond to the PBGs, i.e. to the reflection bands, and the dark regions correspond to the passbands or intraband modes. At normal incidence of the EMWs ( $\theta = 0$ ), the TE- and TM-polarized wave spectra coincide, i.e. degeneracy takes place. At oblique incidence of the EMW ( $\theta \neq 0$ ), the degeneracy of the disappears, as the optical paths of the rays corresponding to the modes of both polarizations become different. The increase of the incidence angle leads to the shift of the PBG and transmission band boundaries towards higher frequencies and to a slight broadening of the PBG for TE-modes and narrowing of the PBG of or the TM-modes. Accordingly, as  $\theta$  increases the TE-mode transmission bands narrow, while the TM-mode transmission bands broaden.

The PBG of the dielectric PC (SiO<sub>2</sub>/TiO<sub>2</sub>)<sup>9</sup> is approximately 4 times wider than the PBG of the bigyrotropic PC (YIG/Bi:YIG)<sup>30</sup> (Figure 2, *a, c* and Figure 2, *b, d*). In the three-periodic  $[(\text{SiO}_2/\text{TiO}_2)^3(\text{YIG}/\text{Bi:YIG})^{10}]^3$  structure, the PBG position is still defined by the dielectric cells, whereby the PBG itself is a little wider than that of the dielectric PC due to the introduction of magnetic cells as can be seen from the comparison of spectra in Figure 2, *a, e* and Figure 2, *b, f*. Moreover, the presence of magnetic cells leads to the appearance of several reflection bands, each of which is split in two (i.e., as shown before in [9], the number of peaks in each band is equal to  $K-1$ , which corresponds to two in this structure).

#### 4.2. Transverse magneto-optic Kerr effect

The influence of the magnetization in YIG and Bi:YIG layers on the optical response of the system is discussed below referring to the reflection and transverse MO Kerr effect spectra. In the following, we focus on the transverse MO Kerr effect in the vicinity of the intraband modes because this effect can achieve high values in the area of spectrally narrow optical resonances (an example of which is the

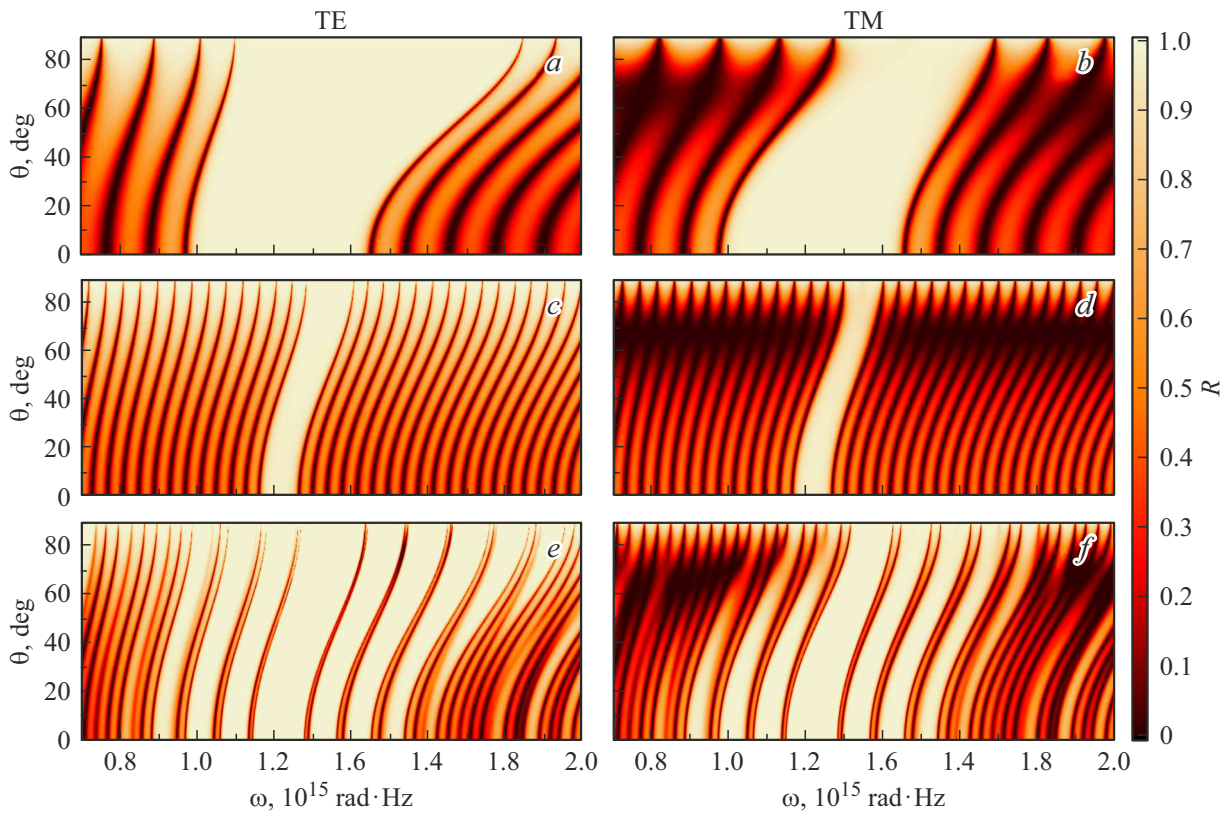


**Figure 2.** Reflection spectra  $R^{\text{TE, TM}}(\omega, \theta)$  for TM- and TE-modes (left and right columns, respectively) for PC with  $N = 3$ ,  $M = 10$ ,  $K = 3$ : (a, b) non-magnetic PC  $[(\text{SiO}_2/\text{TiO}_2)^N]^K$ ; (c, d) magnetic PC  $[(\text{YIG}/\text{Bi}:\text{YIG})^M]^K$ ; (e, f) three-periodic magnetic PC structure  $[(\text{SiO}_2/\text{TiO}_2)^N(\text{YIG}/\text{Bi}:\text{YIG})^M]^K$ . The YIG, Bi:YIG layers are magnetized along the  $y$  axis. The Bragg's wavelengths for the non-magnetic and magnetic cells are equal to  $\lambda_{01} = \lambda_{02} = 1.55 \mu\text{m}$ .

defect modes inside the PBG) [33]. Therefore, for higher contrast of intraband modes the number of superperiods is increased up to  $K = 10$ . Here, the Bragg condition is implemented at the same wavelengths  $\lambda_{01} = \lambda_{02} = 1.582 \mu\text{m}$  for both subcells so that one of the intraband modes (narrow reflection bands) coincides with the operating (telecommunication) wavelength  $\lambda = 1.55 \mu\text{m}$ .

Figure 3 shows the reflection spectra of the  $[(\text{SiO}_2/\text{TiO}_2)^3(\text{YIG}/\text{Bi}:\text{YIG})^{10}]^{10}$  structure (blue and red curves for the magnetization in the bigyrotropic layers along and opposite to the  $y$  axis, respectively) and the transverse MO Kerr effect parameter  $\delta$  (grey curve) calculated using equation (11) for the fixed incidence angle  $\theta = 60^\circ$ . Several intraband modes exist inside the PBG (Figure 3, a), with each of them split into  $(K-1) = 9$  full transmission bands (in a form of „comb“), which corresponds to  $R \rightarrow 0$ . Note that within the graphical accuracy the spectra  $R^+$  and  $R^-$  in Figure 3, a are almost indistinguishable. The split intraband mode spectra in the area of  $\omega = 1.21 \cdot 10^{15} \text{ rad} \cdot \text{Hz}$  are shown in Figure 3, b, and Figure 3, c zoom on one of the reflective minima of the intraband mode at  $\omega = 1.2161 \cdot 10^{15} \text{ rad} \cdot \text{Hz}$  (which corresponds to the wavelength of  $1.55 \mu\text{m}$ ). It can be seen that near the resonant frequency  $\delta \rightarrow \pm 1$ . Such high values of the transverse MO Kerr effect are comparable with  $\delta$

in magneto-plasmonic resonant structures [33]. However, in contrast to magneto-plasmonic structures, the investigated three-periodic magnetic PC system is characterized by negligibly low loss in the near IR range. During magnetization inverse of the bigyrotropic layers, i.e. during rotation of the magnetization vector at  $180^\circ$  with respect to the positive  $y$  axis, blue shift of spectrum takes place and achieves 0.5 GHz (Figure 4, c). The shift of the minimum reflection coefficient position during the magnetization inverse is small with respect to the full width at half maximum of the reflection band itself (FWHM = 50 GHz) for this structure, however, it can be increased in materials with the specific Faraday rotation angle larger than that of YIG. For example, europium sulfide and europium selenide have the potential to replace in the nearest future magnetic garnets in magnetophotonic devices due to the MO constants exceeding the corresponding YIG constants by hundreds of times [43].

Behavior of reflection coefficients during the magnetization inverse of the magnetic layers is discussed below. Figure 4 shows the reflection spectra for TE- (a, b) and TM-waves (c, d) incident on the  $[(\text{SiO}_2/\text{TiO}_2)^3(\text{YIG}/\text{Bi}:\text{YIG})^{10}]^{10}$  structure at  $60^\circ$ . Red (solid) lines show the EMW reflection spectra for the cases of the magnetization of YIG and Bi:YIG layers

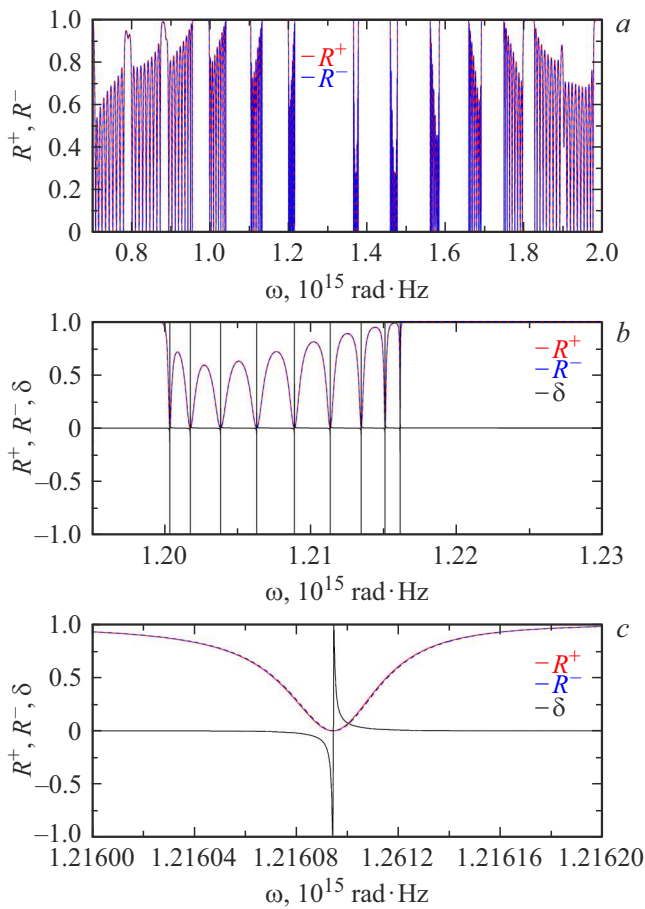


**Figure 3.** The reflection spectra and the MO Kerr effect parameter in the  $[(\text{SiO}_2/\text{TiO}_2)^3(\text{YIG}/\text{Bi:YIG})^{10}]^{10}$  structure for the TE-wave incident at  $\theta = 60^\circ$ . (c, b) — sequential zoom of spectra for the region near  $\omega = 1.2161 \cdot 10^{15}$  rad · Hz (corresponds to the operating wavelength  $1.55 \mu\text{m}$ ). The magnetization of the bigyrotropic layers is oriented along and opposite to the y axis (red solid and blue dashed curves, respectively), the Bragg's wavelengths for the non-magnetic and magnetic cells are  $\lambda_{01} = \lambda_{02} = 1.582 \mu\text{m}$ .

along the y axis, blue (dashed) lines show the reflection spectra for the magnetization opposite to the y axis. The Bragg wavelengths for the cells are selected in order to ensure the narrowest reflection minima at the given operating wavelength  $1.55 \mu\text{m}$  separately for the TE- and TM-modes. This can be clearly seen in Figure 4, a, b which shows the EMW spectra for the magnetic layer thicknesses  $l_{\text{YIG}} = 0.179 \mu\text{m}$ ,  $l_{\text{Bi:YIG}} = 0.164 \mu\text{m}$  (for TE-mode) and  $l_{\text{YIG}} = 0.184 \mu\text{m}$ ,  $l_{\text{Bi:YIG}} = 0.168 \mu\text{m}$  (for TM-mode). It is seen that the rotation of the magnetization vector by  $180^\circ$  relative to the positive direction of the axis y leads to a blue shift of the reflection spectrum. Angular frequency shift of the reflection spectrum during the magnetization inverse (i.e. the difference of reflection coefficient minima) is about  $0.4 \text{ rad} \cdot \text{Hz}$  for the TE-mode (Figure 4, a), and about  $2.4 \text{ rad} \cdot \text{Hz}$  for the TM-mode (Figure 4, b). The value of this shift (i.e. the difference

of reflection minima) during the magnetization inverse of the structure can be varied, for example, by variation of the magnetic layer thicknesses. Figure 4, c, d shows the equivalent spectra for the magnetic layers with increased thickness:  $l_{\text{YIG}} = 1.283 \mu\text{m}$ ,  $l_{\text{Bi:YIG}} = 1.176 \mu\text{m}$  (for the TE-mode) and  $l_{\text{YIG}} = 1.286 \mu\text{m}$ ,  $l_{\text{Bi:YIG}} = 1.179 \mu\text{m}$  (for the TM-mode). Comparison of Figure 4, a and 4, c and Figure 4, b and 4, d shows that for the TE-mode the frequency shift increases by about 6 times, up to  $2.4 \text{ rad} \cdot \text{GHz}$ , and for the TM-modes the frequency shift increase is more than twofold, up to  $5.6 \text{ rad} \cdot \text{GHz}$ . Such noticeable difference in the shift values for the TE- and TM-modes can be explained by considerable difference in the off-diagonal tensor elements  $\hat{\epsilon}$  and  $\hat{\mu}$  (Table).

Note that there is currently a technological constraint in the fabrication of YIG films — usually due to the mismatch strains between the garnet and substrate, garnet films with thicknesses more than  $1.2 \mu\text{m}$  lose their optical quality and can crack. In the investigated PC, the magnetic film thicknesses do not exceed this limit.

## 5. Conclusion

The features of the reflection spectra (in the near IR range) of a three-periodic quaternary PC consisting of nonmagnetic dielectric layers (silicon and titanium oxides) and magnetoactive layers (YIG and Bi:YIG) have been investigated. It has been found that the transverse MO Kerr effect which appears in the investigated structure can reach maximal values ever reported for this effect (values of the „modulation depth“  $\delta \rightarrow \pm 1$ ), which is shown at the frequency corresponding to the telecommunication wavelength  $1.55 \mu\text{m}$ . It is shown that during the  $180^\circ$  - magnetization inverse of the magnetic layers in the structure (along and opposite to the y axis) the reflection minimum shifts in frequency from tenths of GHz to several GHz.

The transverse MO Kerr effect makes it possible to implement a modulation of the shift of the PC transmission/reflection band on the basis of the investigated structure through the magnetization inverse in the magnetoactive layers ( $180^\circ$  turn of the magnetization direction of the layers with respect to the direction perpendicular to the propagation of light). Operating (switching) frequency of such a modulator will be limited by the time of the magnetization inverse of the structure and can achieve values of about of hundreds of MHz [44].

The obtained dependencies can be used for quality control of the PC surface, to get more complete picture of the PC magnetization (i.e. information on the transverse magnetization component in the layers) which cannot be obtained only through the Faraday effect and the polar MO Kerr effect experiments [33]. The results can be also used for the creation of magnetoactive optoelectronic components and nanophotonic devices (modulators and sensors) operating in the IR range. Moreover, the investigated PC can be used to create precision sensors (chemical sensors,

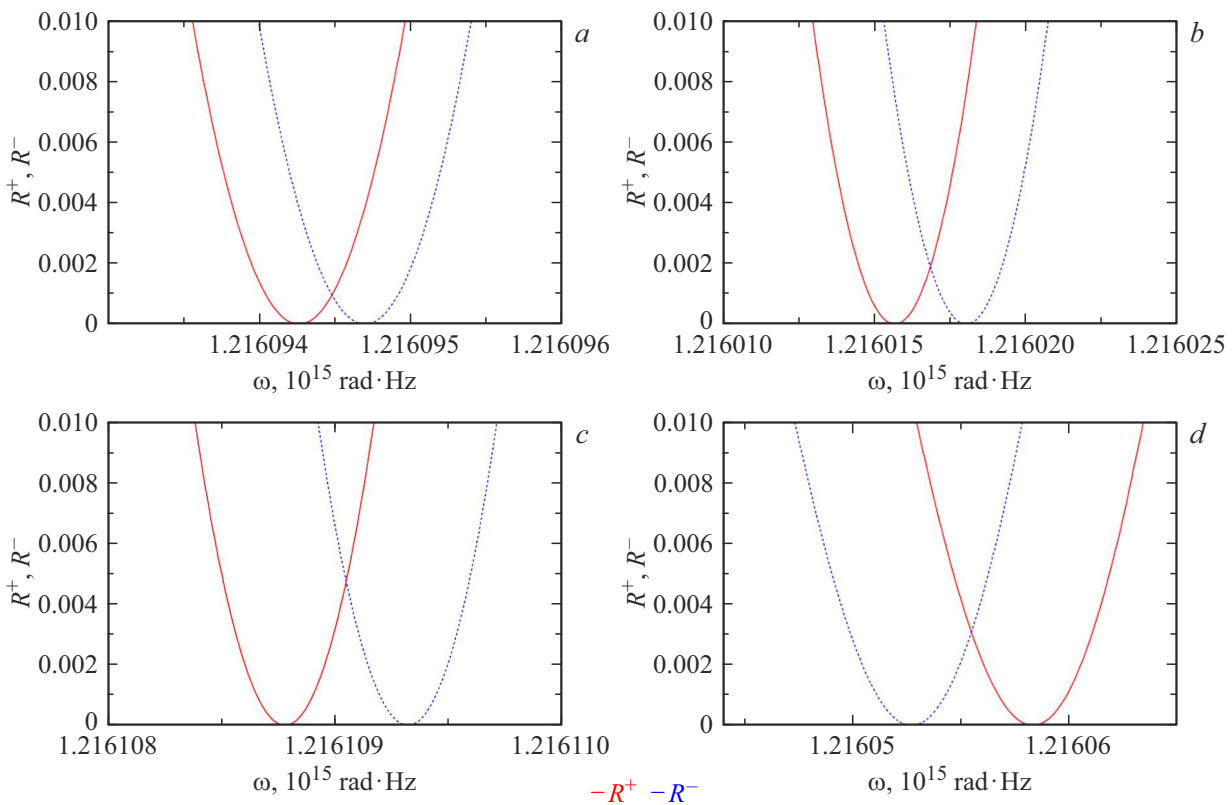


**Figure 4.** Reflection spectra of the TE-wave (*a, b*) and TM-wave (*c, d*) in the same structure as in Figure 3. Wave incidence angle  $\theta = 60^\circ$ . The magnetization vectors in YIG and Bi:YIG are oriented along the  $y$  axis (red solid curves) and opposite to the  $y$  axis (blue dashed curves). The Bragg's wavelengths for the non-magnetic and magnetic cells: (*a*)  $\lambda_{01} = \lambda_{02} = 1.582 \mu\text{m}$ ; (*b*)  $\lambda_{01} = \lambda_{02} = 1.6198 \mu\text{m}$ ; (*c*)  $\lambda_{01} = 1.6132 \mu\text{m}$ ,  $\lambda_{02} = 7\lambda_{01}$ ; (*d*)  $\lambda_{01} = 1.6174 \mu\text{m}$ ,  $\lambda_{02} = 7\lambda_{01}$ .

biosensors) whose operating principle is based on recording the variation of the refractive index of the analytical medium through monitoring the transverse MO Kerr effect [45,46].

## Funding

This study was supported by the Russian Science Foundation (project №. 23-22-00466).

## Conflict of interest

The authors declare that they have no conflict of interest.

## References

- [1] J.D. Joannopoulos, S.G. Johnson, J.N.J. Winn, R.D. Meade. *Photonic Crystals. Molding the Flow of Light*, 2nd ed. (Princeton University Press, Princeton, 2008).
- [2] D. Dzirbou. *Complex Oxide Photonic Crystals*. (Royal Institute of Technology, Stockholm, 2009).
- [3] D.W. Prather, A. Sharkawy, S. Shi, J. Murakowski, G. Schneider. *Photonic crystals: theory, applications, and fabrication*. (John Wiley & Sons, New Jersey, 2009).
- [4] K. Sakoda. *Optical properties of Photonic Crystals*, 2nd ed. (Springer, Berlin, 2005). DOI: 10.1017/CBO9781107415324.004
- [5] V.F. Shabanov, S.Ya. Vetrov, A.V. Shabanov. *Optika fotonnykh kristallov*. (SO RAN, Novosibirsk, 2005).
- [6] I.S. Panyaev, L.R. Yafarova, D.G. Sannikov, N.N. Dadoenkova, Y.S. Dadoenkova, I.L. Lyubchanskii. *J. Appl. Phys.*, **126** (10), 103102 (2019). DOI: 10.1063/1.5115829
- [7] I.S. Panyaev, N.N. Dadoenkova, Y.S. Dadoenkova, I.A. Rozhleys, M. Krawczyk, I.L. Lyubchanskii, D.G. Sannikov. *J. Phys. D. Appl. Phys.*, **49** (43), 435103 (2016). DOI: 10.1088/0022-3727/49/43/435103
- [8] I.S. Panyaev, D.G. Sannikov, Yu.S. Dadoenkova, N.N. Dadoenkova. *IEEE Sens. J.*, **22** (23), 22428 (2022). DOI: 10.1109/JSEN.2022.3217117
- [9] I.S. Panyaev, D.G. Sannikov, N.N. Dadoenkova, Yu.S. Dadoenkova. *Appl. Opt.*, **60** (7), 1943 (2021). DOI: 10.1364/ao.415966
- [10] I.A. Glukhov, S.G. Moiseev. *Opt. i spektr.*, **131** (11), 1475 (2023) (in Russian). DOI: 10.61011/OS.2023.11.57005.5095-23
- [11] J.W. Kos, M. Krawczyk, Yu.S. Dadoenkova, N.N. Dadoenkova, I.L. Lyubchanskii. *J. Appl. Phys.*, **115** (17), 174311 (2014). DOI: 10.1063/1.4874797
- [12] Yu.S. Dadoenkova, N.N. Dadoenkova, I.L. Lyubchanskii, J.W. Klos, M. Krawczyk. *J. Appl. Phys.*, **120** (7), 73903 (2016). DOI: 10.1063/1.4961326
- [13] J.W. Klos, M. Krawczyk, Yu.S. Dadoenkova, N.N. Dadoenkova, I.L. Lyubchanskii. *IEEE Trans. Magn.*, **50** (11), 2 (2014). DOI: 10.1109/TMAG.2014.2321532

- [14] Yu.S. Dadoenkova, N.N. Dadoenkova, J.W. Klos, M. Krawczyk, I.L. Lyubchanskii. *Phys. Rev. A*, **96** (4), 43804 (2017). DOI: 10.1103/PhysRevA.96.043804
- [15] Yu.S. Dadoenkova, N.N. Dadoenkova, I.L. Lyubchanskii, J.W. Klos, M. Krawczyk. *IEEE Trans. Magn.*, **53** (11), 1 (2017). DOI: 10.1109/TMAG.2017.2712278
- [16] E.E. Narimanov. *Phys. Rev. X*, **4** (4), 1 (2014). DOI: 10.1103/PhysRevX.4.041014
- [17] V.N. Smolyaninova, B. Yost, D. Lahnehan, E.E. Narimanov, I.I. Smolyaninov. *Sci. Rep.*, **4** (1), 5706 (2015). DOI: 10.1038/srep05706
- [18] S.V. Zhukovsky, A.A. Orlov, V.E. Babicheva, A.V. Lavrinenko, J.E. Sipe. *Phys. Rev. A — At. Mol. Opt. Phys.*, **90** (1), 013801 (2014). DOI: 10.1103/PhysRevA.90.013801
- [19] A.V. Chebykin, V.E. Babicheva, I.V. Iorsh, A.A. Orlov, P.A. Belov, S.V. Zhukovsky. *Phys. Rev. A*, **93** (3), 033855 (2016). DOI: 10.1103/PhysRevA.93.033855
- [20] N.N. Dadoenkova, Y.S. Dadoenkova, I.S. Panyaev, D.G. Sannikov, I.L. Lyubchanskii. *J. Appl. Phys.*, **123** (4), 043101 (2018). DOI: 10.1063/1.5011637
- [21] D.M. El-Amassi, S.A. Taya, D. Vigneswaran. *J. Theor. Appl. Phys.*, **12** (4), 293 (2018). DOI: 10.1007/s40094-018-0308-x
- [22] J. Wu, J. Gao. *J. Supercond. Nov. Magn.*, **28** (7), 1971 (2015). DOI: 10.1007/s10948-015-3002-0
- [23] S.M. Lo, S. Hu, G. Gaur, Y. Kostoulas, S.M. Weiss, P.M. Fauchet. *Opt. Express*, **25** (6), 7046 (2017). DOI: 10.1364/oe.25.007046
- [24] S.M. Aminifard, M. Sovizi. *Opt. Commun.*, **322**, 1 (2014). DOI: 10.1016/j.optcom.2014.01.086
- [25] O.V. Borovkova, H. Hashim, M.A. Kozhaev, S.A. Dagesyan, A. Chakravarty, M. Levy, V.I. Belotelov. *Appl. Phys. Lett.*, **112** (6), 063101 (2018). DOI: 10.1063/1.5012873
- [26] A.K. Zvezdin, V.A. Kotov. *Modern Magneto-optics and Magneto-optical Materials*. (IOP Publishing, Bristol and Philadelphia, 1997). DOI: 10.1887/075030362X
- [27] J. Qin, S. Xia, W. Yang, H. Wang, W. Yan, Y. Yang, Z. Wei, W. Liu, Y. Luo, L. Deng, L. Bi. *Nanophotonics*, **11** (11), 2639 (2022). DOI: 10.1515/nanoph-2021-0719
- [28] Yu.S. Dadoenkova, F.F.L. Bentivegna, N.N. Dadoenkova, I.L. Lyubchanskii. *J. Opt.*, **19** (1), 15610 (2016). DOI: 10.1088/2040-8986/19/1/015610
- [29] V.I. Belotelov, A.K. Zvezdin. *J. Opt. Soc. Am. B*, **22** (1), 286 (2005). DOI: 10.1364/JOSAB.22.000286
- [30] D. Sylgacheva, N. Khokhlov, A. Kalish, S. Dagesyan, A. Prokopov, A. Shaposhnikov, V. Berzhansky, M. Nur-E-Alam, M. Vasiliev, K. Alameh, V. Belotelov. *Opt. Lett.*, **41** (16), 3813 (2016). DOI: 10.1364/OL.41.003813
- [31] M. Inoue, T. Fujii. *J. Appl. Phys.*, **81** (8 PART 2B), 5659 (1997). DOI: 10.1063/1.364687
- [32] D.W. Berreman. *J. Opt. Soc. Am.*, **62** (4), 502 (1972). DOI: 10.1364/JOSA.62.000502
- [33] O.V. Borovkova, F. Spitzer, V.I. Belotelov, I.A. Akimov, A.N. Poddubny, G. Karczewski, M. Wiater, T. Wojtowicz, A.K. Zvezdin, D.R. Yakovlev, M. Bayer. *Nanophotonics*, **8** (2), 287 (2019). DOI: 10.1515/nanoph-2018-0187
- [34] O. Borovkova, A. Kalish, V. Belotelov. *Opt. Lett.*, **41** (19), 4593 (2016). DOI: 10.1364/ol.41.004593
- [35] J.R. Devore. *J. Opt. Soc. Am.*, **41** (6), 416 (1951). DOI: 10.1364/JOSA.41.000416
- [36] I.H. Malitson. *J. Opt. Soc. Am.*, **55** (10), 1205 (1965). DOI: 10.1364/JOSA.55.001205
- [37] B. Johnson A.K. Walton. *Br. J. Appl. Phys.*, **16** (4), 475 (1965). DOI: 10.1088/0508-3443/16/4/310
- [38] M. Wallenhorst, M. Niemoller, H. Dotsch, P. Hertel, R. Gerhardt, B. Gather. *J. Appl. Phys.*, **77** (7), 2902 (1995). DOI: 10.1063/1.359516
- [39] P. Hansen, J.P. Krumme. *Thin Solid Films*, **114** (1), 69 (1984). DOI: 10.1016/0040-6090(84)90337-7
- [40] M. Torfeh, H. Le Gall. *Phys. Status Solidi*, **63** (1), 247 (1981). DOI: 10.1002/pssa.2210630133
- [41] J.P. Krumme, C.P. Klages, V. Doormann. *Appl. Opt.*, **23** (8), 1184 (1984). DOI: 10.1364/AO.23.001184
- [42] N.N. Dadoenkova, I.L. Lyubchanskii, M.I. Lyubchanskii, E.A. Shapovalov, Y.P. Lee. *Frontiers in Optical Technology: Materials & Devices* (Nova Science, New York, 2007), p. 22–72.
- [43] R. Sobolewski, J.R. Park. *IEEE Trans. Appl. Supercond.*, **11** (11), 727 (2001). DOI: 10.1109/77.919448
- [44] V.V. Randoshkin, A.Ya. Chervonenkis. *Prikladnaya magnitooptika* (Energoatomizdat, Moskva, 1990) (in Russian).
- [45] M. Amanollahi, M. Zamani. *Phys. Scr.*, **98** (8), 85505 (2023). DOI: 10.1088/1402-4896/ACE087.
- [46] L. Li, F. Lei, X. Zong, P. Li, Y. Liu. *Results Phys.*, **51**, 106640 (2023). DOI: 10.1016/J.RINP.2023.106640

Translated by E.Ilinskaya